Available online at www.sciencedirect.com
SCIENCE DIRECT®
Journal of Volcanology and Geothermal Research 139 (2005) 241–258
Journal of volcanology and geothermal research
www.elsevier.com/locate/jvolgeores

Classification and idealized limit-equilibrium analyses of dome collapses at Soufrière Hills volcano, Montserrat, during growth of the first lava dome: November 1995–March 1998

John Simmons[1], Derek Elsworth*, Barry Voight

College of Earth and Mineral Sciences, Penn State University, University Park, PA 16802, United States

Received 17 December 2003; accepted 5 August 2004

Abstract

Styles of dome collapse at Soufrière Hills volcano (SHV; November 1995–March 1998) are classified by relations between extrusion rate prior to collapse and collapse volume. Four separate modes of collapse behavior are apparent. Notably, moderate rates of extrusion are shown to result in two disparate modes of collapse: small-to-large collapses on steeply inclined failure planes that switch to collapse volumes an order of magnitude larger that cut deeply into the dome core. For constant effusion rates, this bifurcation in behavior is explained by the monotonic growth of a soft core that ultimately promotes the development of a deep-seated failure over previously favored shallow failure modes. Models are developed to test this hypothesis that first constrain magnitudes of cohesive and frictional strength with observed dome collapse morphologies and volumes. Evaluations of dome strengths confirm the important role of a soft core in promoting deep failure. A nested model representing a cohesive dome core, surrounded by a frictional rind, with constant rate of magma input, confirms the observed bifurcation in behavior, and for invariant effusive activity. Importantly, failure volumes are shown to increase by close to an order of magnitude for a few percent change in the proportion of dome core comprising cohesive material. This model is capable of replicating, a posteriori, the approximate timing of failure for both small (250 m) and large (325 m) domes. The timing and style of the 17 September 1996 and June to November 1997 collapses are honored.

Keywords: lava dome; collapse; pyroclastic flows; bifurcation

1. Introduction

The collapse of lava domes is a complex and hazardous phenomenon. Associated threats include generation of pyroclastic flows, the triggering of subsequent explosive activity that may generate

* Corresponding author. Fax: +1 814 865 3248.
E-mail addresses: john.r.simmons@exxonmobil.com (J. Simmons), elsworth@psu.edu (D. Elsworth), voight@ems.psu.edu (B. Voight).
[1] Current affiliation: ExxonMobil Exploration Company, 233 Benmar, Houston, TX 77060.

0377-0273/$ - see front matter © 2004 Elsevier B.V. All rights reserved.
doi:10.1016/j.jvolgeores.2004.08.009

column-collapse pyroclastic flows and widespread ashfall, and the elevated potential for lahars. Erosion of the carapace, disturbance of the talus shield providing support for dome lava, and internal dome forces, especially for the gas-infused Peléan-type domes, are important contributors to collapse. Potential mechanisms for these failures include thrust forces or mass weakness associated with an active lava lobe intrusion or extrusion (Calder et al., 2002; Watts et al., 2002; Voight et al., 2002), slope oversteepening by erosion and piping (Voight and Elsworth, 1997; Fink and Griffiths, 1998; Sparks et al., 2000), generation of fluid overpressurization of a weak underlying stratum (Lopez and Williams, 1993; Voight and Elsworth, 1997; Crowley and Zimbelman, 1997; Watters et al., 2000), the driving of thermal fractures through the brittle rind (Yamasato et al., 1998), rainwater vaporization-induced overpressurization of the outer dome (Matthews and Barclay, 2004; Simmons et al., 2004; Elsworth et al., in press), and gas overpressurization of the inner dome itself (Voight and Elsworth, 2000; Elsworth and Voight, 2001).

The andesite lava dome of Soufrière Hills volcano (SHV), Montserrat, B.W.I., evolved through several eruptive styles from November 1995 to March 1998, each associated with a particular style of dome collapse. A small overall dome volume, relatively low extrusion rate and relatively low collapse volume marked the early stage collapses of 1996. Later stage higher-volume collapses of 1997 resulted in violent explosions. Each style conforms to a systematic pattern of extrusion rate and associated collapse volume.

The following provides a classification of dome collapse styles during times of active lava effusion based on the dome volume involved. Collapse styles evolve from relatively innocuous small-to-large failures, to dangerous and potentially explosive major failures. All collapse volumes 0–4×10^6 m^3 Dense Rock Equivalent (DRE) are referred to as small-to-large collapses, those with volumes of 4–20×10^6 m^3 DRE are termed major collapses, and collapses involving greater than 20×10^6 m^3 DRE are termed gigantic collapses (after Calder et al., 2002); all subsequent volumes will be referred to in terms of DRE (Calder et al., 2002).

Behavioral signatures are identified for particular collapse styles of SHV that can aid (and indeed have aided) in risk assessments, both on Montserrat and at similar andesite domes elsewhere. These observations of collapse are supported by a simplified dual-region limit-equilibrium model of the dome. The simple first-order model incorporates a cohesive volatile-rich core encapsulated by a primarily frictional, degassed rind. Feasible rock mass strengths are defined by back analysis, to provide a consistent suite of frictional and cohesive strengths for the dual regions. The model is applied to a growing dome to define the self-organized change in collapse style as failure mode bifurcates from initial shallow surface spalling to switch to a deep-seated failure that cuts more deeply into the dome core. Importantly, this occurs as a sudden switch from shallow to deep, rather than as a progressive deepening of the initial shallow failures. This behavior is followed to define the style and approximate timing of major failures in both relatively small (r=250 m) and large (r=325 m) domes. The model is subsequently modified to incorporate retrogressive failure, an alternative mechanism for the development of major failures, in an effort to explain long-duration major collapses, e.g., the c. 9-h collapse on 17 September 1996.

2. Collapse styles

A variety of styles have been apparent in the episodic dome collapses observed at SHV in the period November 1995 to March 1998 (Watts et al., 2002; Calder et al., 2002). They have ranged from shallow, small-to-large collapses with relatively low mobility, to energetic major collapses that have spontaneously developed into long-runout pyroclastic flows. One method of classifying these failures is by collapse size, e.g., small-to-large/major/gigantic. Another classification method is to consider the relationship between collapse volume and extrusion rate. Extrusion rate and collapse volume data for 22 collapses recorded in the period 29 July 1996 to 26 December 1997 (Table 1 of Calder et al., 2002) are plotted in Fig. 1. In a general sense, extrusion rates and collapse volumes are positively correlated; larger extrusion rates result in larger volumes of unstable material being available to both drive and to participate in the collapse. Unfortunately, this simplistic observation is confounded by the presence of a small number of outlier major collapses that have occurred while preceding extrusion rates remain low.

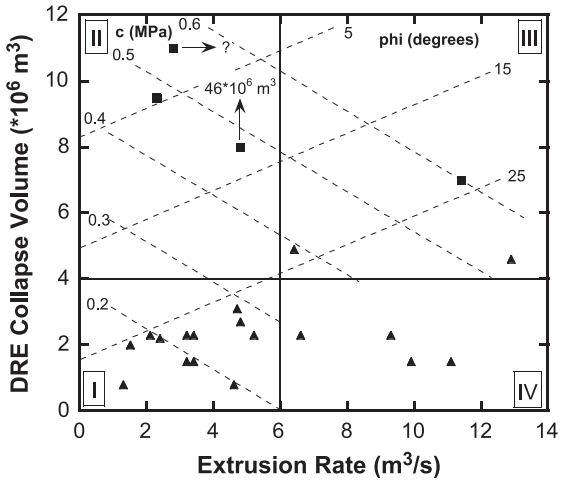

Fig. 1. Dome collapse patterns for the period July 1996 to December 1997 (i.e., all collapses of the first lava dome) based on extrusion rate prior to collapse and corresponding collapse volume (data from Calder et al., 2002; Table 1). Both collapses resulting in explosive activity (■) and those not (▲) are included. Feasible strengths obtained from back analyses demonstrate the increasing dominance of cohesion with increasing collapse volume. *Quadrant I*: early stage dome growth, small-to-large collapses (July–early September 1996 and March–April 1997) termed Type I collapses. *Quadrant II*: major dome collapses (17 September 1996) termed Type II collapses. *Quadrant III*: major dome collapses associated with rapid extrusion rates. *Quadrant IV*: small-to-large dome collapses associated with low viscosity lava with a 'pancake-like' morphology (January 1997) termed Type IV collapses.

Linking this progression of collapse modes to an invariant input of fresh magma to the dome is the focus of this work. Four principal styles of dome collapse are suggested based on the quadrants of Fig. 1, defining collapses as either small-to-large or major in size, and resulting from either slow-to-moderate (<6 m^3/s) or fast (≥6 m^3/s) extrusion rates. These broad divisions provide some basis for understanding the fundamental mechanisms that ultimately drive failure.

2.1. Small-to-large collapses at slow-to-moderate extrusion rate

Slow-to-moderate extrusion rate/small-to-large volume collapses, here termed Type I collapses (Quadrant I of Fig. 1), tended to occur during the lower overall volume (20–45×10^6 m^3 DRE) stages of dome development (e.g., Fig. 2a), i.e., July to early September 1996 and March to April 1997 (Calder et al., 2002). Despite the low volume of the dome, the small-to-large failures are typically restricted to high-angle collapses, incapable of transecting the dome and unroofing the interior system, thus diminishing the potential for explosive eruption (Robertson et al., 2000). This style of dome collapse has predominated during periods of low background extrusion rate.

2.2. Major collapses at slow-to-moderate extrusion rate

Slow-to-moderate extrusion rate/major collapses (e.g., Fig. 2b), here termed Type II collapses (Quadrant II of Fig. 1), are difficult to explain in terms of a direct progression from Type I collapses. This style corresponds to the 17 September 1996 collapse, which lasted c. 9 h and removed c. 35% of the dome (Calder et al., 2002) resulting in sub-Plinian explosive activity (Robertson et al., 1998). Seven collapses occurred between 29 July and 3 September 1996; dome materials were necessarily weak relative to the topographic setting and stresses, such that instability was essentially the norm for that period. Considering this, only subtle deviations from this norm occurred in the period just prior to 17 September 1996. Extrusion rate (~2–3 m^3/s) and overall dome volume (~26–27×10^6 m^3) stayed relatively constant during the 2 weeks preceding the collapse (Calder et al., 2002). However, cyclic deformation (Voight et al., 1998) and hybrid earthquake swarms (Robertson et al., 1998) increased during the 2-week precollapse period, and increased steam and ash venting were observed (McGuire et al., 1996).

The collapse of 21 September 1997 occurred with the invigorated onset of a new ~7-week cycle (Voight et al., 1998), so it is a question of whether the extrusion rate to apply was that associated with the new cycle, or the sluggish end of the previous cycle. An arrow on the point in Fig. 1 indicates that the relevant rate might be larger. The gigantic collapse on 26 December (Boxing Day) 1997 is also represented with an arrow on the point, indicating that its collapse volume (~46×10^6 m^3) is considerably higher than the scale of Fig. 1. This failure, reviewed extensively in Voight et al. (2002), was the final and largest collapse event of the first SHV lava dome. It may be considered an extension of Type II behavior for the purposes of this "first approximation" classification scheme.

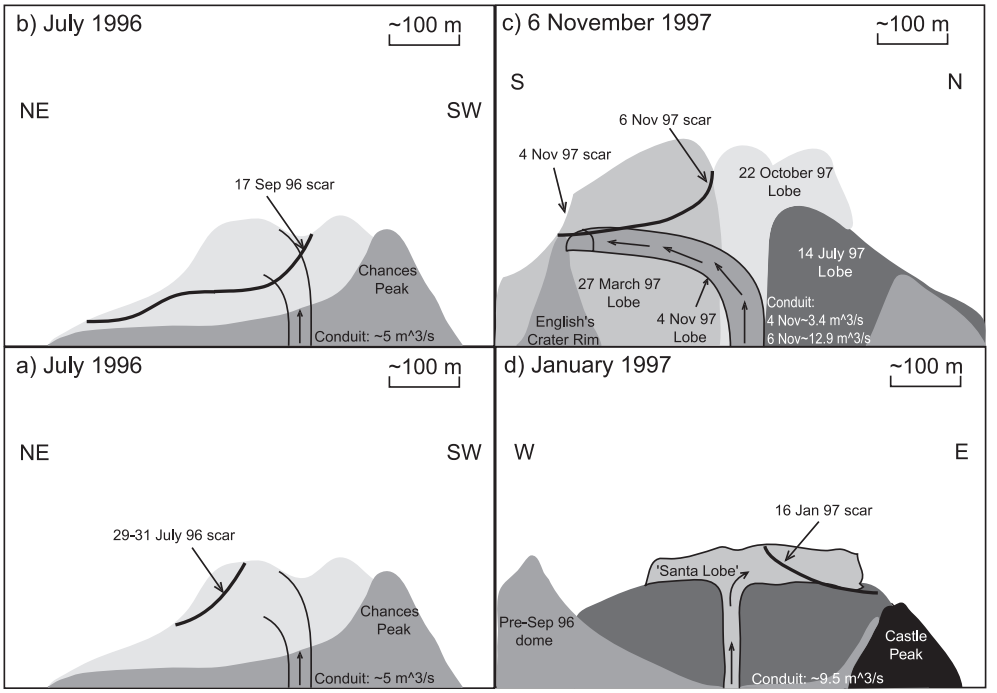

Fig. 2. Cartoons of approximate dome profiles and collapse scars corresponding to the various collapse types identified in Fig. 1 (after Watts et al., 2002). (a) July 1996: the 29–31 July scar corresponds to a Type I failure. (b) July 1996: the 17 September scar corresponds to a Type II failure. (c) November 1997: the 4 November scar corresponds to a Type I failure, and the 6 November scar corresponds to a Type III failure. (d) January 1997: the 16 January scar corresponds to a Type IV failure.

2.3. Major collapses at fast extrusion rate

Classified here as Type III collapses, these failures are better understood than the preceding Type II collapses (Quadrant III of Fig. 1). Type III collapses represent the period from June to November 1997 (Fig. 2c) when major collapses again unroofed the conduit resulting in explosive eruptions (Druitt et al., 2002). From March to April 1997, extrusion rates were quite low (c. 1–3 m^3/s), and rather abruptly in June, the rate increased to c. 6 m^3/s. Between 11 April and 25 June 1997, the total dome volume increased by c. 60% from 43 to 68×10^6 m^3 DRE (Calder et al., 2002).

2.4. Small-to-large collapses at fast extrusion rate

These rather unusual failures are termed Type IV collapses (Quadrant IV of Fig. 1), and could be viewed as an extension of Type III failures. Although collapse volumes are lower than Type III behavior, the failures were morphologically distinct. All four of these collapses occurred during January 1997 when the so-called ‘Santa lobe’ failed successively (Fig. 2d). This lobe was morphologically similar to a pancake that initially extruded and spread symmetrically, indicating a weak, very low viscosity material relative to previous lobes (Watts et al., 2002). These properties are commensurate with the fast extrusion rates, which minimized the opportunity for melt water loss and crystallization inside the conduit. Failures of this nature can be expected when low viscosity lava freely and rapidly extrudes, spreading laterally rather than building vertically.

3. Strength distributions and potential failure mechanisms

Changes in the observed modes of failure may be linked to fundamental differences in the physical

characteristics of the dome, and their evolution in time. Magma transport within the conduit and through the solidifying dome is strongly controlled by increases in viscosity that accompany degassing and crystallization of microlites. Degassing also influences strength of the resulting dome pile, with the highly crystalline magma becoming less cohesive and more frictional as it both degasses and cools. The rates of strength gain, the possible transition from dominantly cohesive to frictional strengths, and the distribution of these predominant strength modes within the dome and its carapace are not well constrained. However, broad estimates for the magnitude of dome strength may be determined from the back analysis of observed failures.

Estimates of feasible cohesion, c, and friction angle, φ, pairs were determined from back analyses of circular failure surfaces in dry rock slopes (Hoek and Bray, 1981), assuming that the influence of interior fluid pressures are minimal. The back analyses were performed to identify minimum strength magnitudes necessary to support precollapse slope angles and heights. The resulting magnitudes of cohesion and friction angle pairs span the range 0–1.1 MPa and 0–45°, respectively, and represent a broad spectrum of material types from viscous magma to solidified lava.

With this broad range of strength pairs defined that prescribe at least minimally stable slopes, the strength distribution was further narrowed (c–φ pairs of 0.2 MPa–25° to 0.6 MPa–5°, see Fig. 4) by requiring that failure predictions should additionally honor observed collapse volumes and failure plane inclinations. This was completed by applying the broad range of strength pairs to a limit-equilibrium analysis of a homogeneous hemispherical lava dome (Eq. (1)) that has been successfully applied to the study of lava dome collapse driven by interior gas overpressures (Voight and Elsworth, 2000; Elsworth and Voight, 2001). Dome profiles from Montserrat Volcano Observatory (MVO) digital elevation maps (DEMs; July–September 1996), Fig. 6 (March–April 1997) of Calder et al. (2002), and Fig. 24 (June–November 1997) of Watts et al. (2002) provide general slope heights and inclinations for the back analyses. The Type IV collapses of January 1997 are omitted as the pancake lobe morphology does not conform to the hemisphere model.

The factor of safety, F_S, is determined for an idealized homogeneous hemispherical lava dome (Fig. 3) of outer radius r with a failure plane inclined at angle α that intersects the toe of the slope, as (Elsworth and Voight, 2001):

$$F_S = \frac{cA + W\cos(\alpha)\tan(\varphi)}{W\sin(\alpha)}, \tag{1}$$

where A is the contact area of the basal detachment plane given as:

$$A = \pi r^2 \cos^2(\alpha), \tag{2}$$

and W is the weight of the block. The failure block weight is evaluated through its volume, V, and unit weight, γ_R, as:

$$W = \gamma_R V, \tag{3}$$

where

$$\begin{aligned} V &= \pi \int_{r\sin\alpha}^{r} (r^2 - y^2)\mathrm{d}y \\ &= \pi r^3 \left[-\frac{2}{3} - \sin(\alpha)\left(1 - \frac{1}{3}\sin^2(\alpha)\right)\right]. \end{aligned} \tag{4}$$

Appropriate strength magnitudes for specific events are constrained by the failure plane inclination required for a particular collapse volume to be removed via Eq. (4). The resulting magnitudes of c–φ pairs (Fig. 4) that represent the individual collapse events of Fig. 1 are linked, enabling the distribution of critical strength parameters to be overprinted on the demarcation of collapse styles discussed previously.

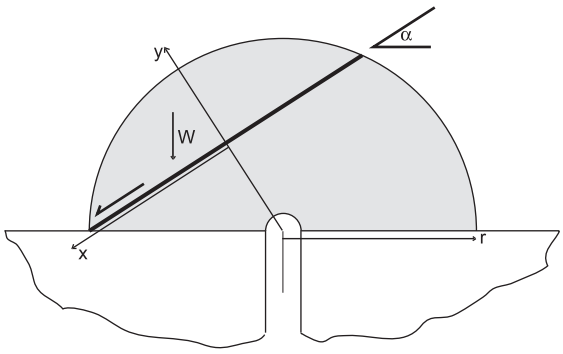

Fig. 3. Schematic diagram of an idealized homogeneous hemispherical lava dome used to constrain appropriate dome rock mass strength distributions for Types I–III failures.

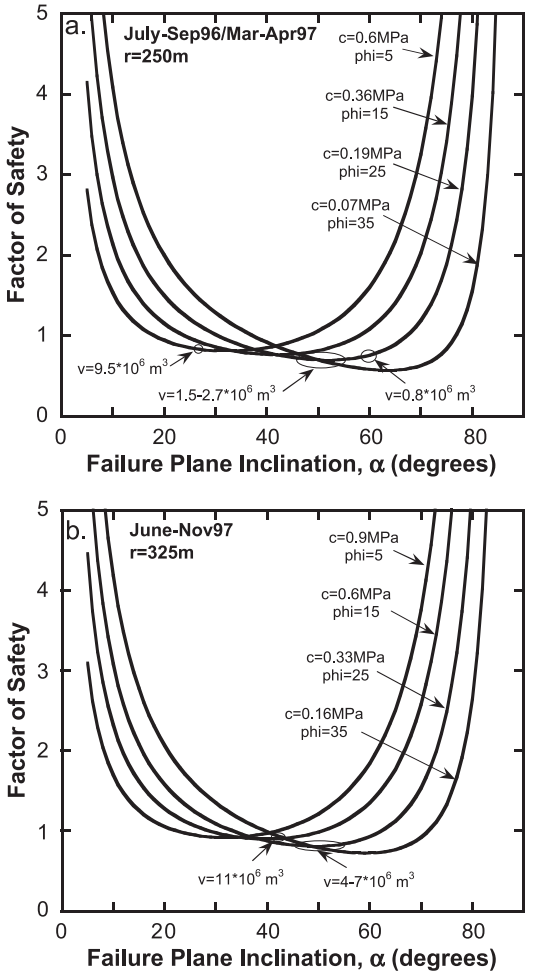

Fig. 4. Factor of safety vs. failure plane inclination plots for hemispherical lava domes using c–φ pairs from back analyses (Hoek and Bray, 1981). Collapse volumes of specific events constrain appropriate c–φ pairs via the failure plane inclination required for that collapse volume. Dome rock density of 2600 kg/m^3 is assumed. (a) Type I and II collapses: slope height of 150 m and inclination of 45° used in back analysis (MVO DEMs and Calder et al., 2002). Dry lava dome and an external dome radius of 250 m (in the hemispherical model) are assumed. (b) Type III collapses: slope height of 200 m and inclination of 52° (Watts et al., 2002) are used in the back analysis and an external dome radius of 325 m is assumed in the hemispherical model.

Fig. 4a represents the periods of July to September 1996 and March to April 1997 when SHV's mean dome radius was of the order of 250 m (Table 1 and Fig. 6 of Calder et al., 2002). Apparent from Fig. 4a are two possible c–φ pairs for the observed small-to-large (0.8–2.7×10^6 m^3) and major failures (9.5×10^6 m^3): 0.2 MPa–25° and 0.6 MPa–5°, respectively. Fig. 4b corresponds to the June to November 1997 time period, when the dome was considerably larger with an approximate radius of 325 m (Table 1 of Calder et al., 2002; Fig. 24 of Watts et al., 2002). Again, two possible c–φ pairs are evident for the collapses of 4–7×10^6 m^3 and 11×10^6 m^3: 0.33 MPa–25° and 0.6 MPa–15°, respectively. Clearly, in all time periods considered, cohesive dominance increases with increasing collapse volume.

This generalization is used to contour rough cohesive and frictional strength trends on Fig. 1. As the strength of the dome becomes on average predominantly more cohesive, the potential to develop deep-seated major failures prevails. As the frictional component dominates, high-angle, small-to-large failures become the dominant mode of collapse. This switch in behavior is supported by observations at Soufrière Hills volcano.

3.1. High-angle gravitational failures

Small-to-large collapses occur in the outer rind of the dome where the older, more degassed and crystalline rocks are predominantly frictional. When cohesion is low and approaches zero, block weight becomes insignificant in driving failure, and the factor of safety is approximated as $\tan(\varphi)/\tan(\alpha)$. Thus, when the failure plane inclination exceeds the friction angle, high-angle, low-volume failure results (Fig. 4a). Type I failures demonstrate this type of behavior, where lava effusion is slow, building a degassed rind in the absence of intense hybrid earthquake swarms.

3.2. Deep-seated failures

The increased hybrid earthquake activity, interpreted to indicate migration of high-pressure gases (Sparks and Young, 2002), and steam and ash venting in the period leading up to the 17 September 1996 (Type II) collapse indicate an increase in interior gas pressurization. Deep-seated failures plausibly occur in bodies dominated by cohesive strength (Figs. 1 and 4) where the downslope component of block weight is large enough to overcome resisting forces. By reducing the frictional strength of the dome to the point of cohesive dominance, interior gas pressuriza-

tion on the order of 10±5 MPa is capable of driving deep failure in hemispherical lava domes (Elsworth and Voight, 2001).

For the Type III collapses, the rapid extrusion rate suggests that two end-member mechanisms are feasible in that (1) lava moving more rapidly does not possess as much time to exsolve volatiles during ascent, meaning that the dome is likely gas pressurized, and (2) injections of the less viscous volatile-rich (cohesive) magma causes weakening and local oversteepening of the heterogeneous dome. Further supporting the theory of interior gas pressurization are the occurrences of cyclic tilt and hybrid earthquake activity preceding Type III collapses (Voight et al., 1998). Either the presence of cohesion dominant lava high in the dome or the occurrence of internal gas overpressurization may provide the strength reduction necessary to result in deep-seated, conduit exposing failures (Elsworth and Voight, 2001; Elsworth et al., in press).

4. Stability models

With strength trends and collapse styles discussed, theoretical stability models logically follow. The stability of lava domes, ignoring external collapse triggers, such as rainfall-induced overpressures, depends upon strength magnitudes and distributions within the dome, failure surface geometry, extent and composition, failure block weight, and possibly the influence of magma movement, internal gas pressurization, and seismic acceleration. Because the exact system parameters are impossible to constrain, an analytical approach is employed. An idealized hemispherical model is suggested in the following, and its limiting equilibrium provides good correlation between observed styles and timing of collapses at SHV. In addition, some retrogressive limit-equilibrium failure models are suggested in order to account for longer duration failures, such as the one that occurred on 17 September 1996.

4.1. Nested model

Excluding the Type IV collapses, Fig. 1 illustrates the requirement for a decreasingly frictional failure surface with increasing collapse volume for a given extrusion rate. Observations at SHV indicate the possibility of internal gas pressurization as a source of both driving forces and cohesive strength dominance (Elsworth and Voight, 2001; Elsworth et al., in press). Complementary to the internal gas pressurization model of Elsworth and Voight (2001), and in compliance with the aforementioned strength trend prerequisite, an idealized dual region hemispherical lava dome model (after Iverson, 1990; Hale and Wadge, 2003) is proposed to replicate Types I–III failures: a primarily cohesive (volatile-rich) hemispherical core of radius b surrounded by a primarily frictional (degassed) rind of outer radius r (Fig. 5). This involves two main simplifications. (1) The core and rind are each modeled as homogeneous entities

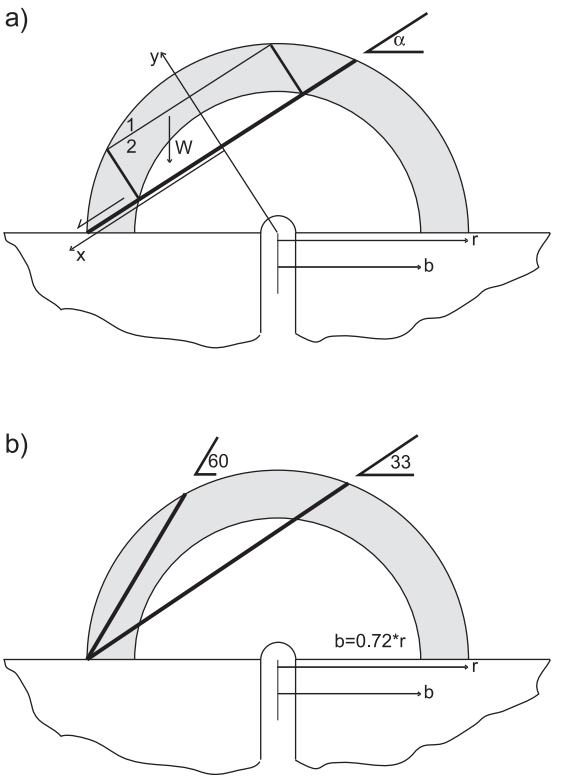

Fig. 5. (a) Schematic diagram of an idealized dual-region hemispherical lava dome with a purely cohesive, volatile-rich, hemispherical core (white) of radius b surrounded by a primarily frictional degassed rind (gray) of radius r. (b) Schematic of potential low and high failure plane orientations in a dome with 37–38% core by volume. The low angle (33°) plane transects the core indicating a high probability of explosive activity following collapse.

when in reality they are both likely to contain significant inhomogeneities. Unfortunately, few data exist to characterize their internal strength and structure, and thus back analysis yields an aggregate behavior that incorporates both size effects and the role of inhomogenieties within the dome. Clearly more elaborate models can be prescribed to represent this observed response, but their constituent properties remain speculative given available data. (2) Although talus generally rings the base of a lava dome, its mechanical effects are ignored here in order to simplify the treatment of the problem. This simplification is somewhat crude, but it seems reasonable (Iverson, 1990) because talus slopes are generally inclined at the angle of repose. They will therefore fail upon the application of an outward, steepening force. Consequently, the outward weight component of a failing block within the quasi-hemispherical dome structure would likely be little inhibited by the talus material.

This representation explains how both small-to-large and major failures occur. Small-to-large failures, according to this "first approximation" model, must result from high failure plane inclinations in order to remove sufficiently low amounts of material, thus relegating them to the frictional rind and obeying the trend of Fig. 1. Conversely, major failures must either occur as singular movements on failure planes inclined much lower where the failure plane transects a large proportion of the cohesive core, or result from the slow retrogression of a series of Type I failures, gradually increasing the cohesive dominance of the failure surface, again satisfying the trend illustrated in Fig. 1. Strength magnitudes of the two regions are chosen in order to best replicate the desired behavior described above, and they are loosely based upon the back analysis performed here. They also agree well with previous dome rock strength estimates from Elsworth and Voight (2001) and Voight and Elsworth (2000). The resulting roughly prorated strengths are c=0.4 MPa; φ=0 and c=0.2 MPa; φ=45° for the core and rind, respectively. The factor of safety for singular planar failures is calculated by modifying Eq. (1) to include the two strength zones as:

$$F_S = \frac{[c_C A_C] + [c_R A_R + W_R \cos\alpha \tan\varphi_R]}{(W_C + W_R)\sin\alpha}, \tag{5}$$

where the subscripts C and R, respectively, correspond to core and rind. The failure surface areas of the core and rind are:

$$A_C = \pi\left(b^2 - r^2\sin^2\alpha\right) \tag{6}$$

and

$$A_R = A - A_C. \tag{7}$$

The corresponding weight of material overlying the core is evaluated through two volumetric regions: (1) a cap, V_{cap}, that overlies a (2) cylindrical portion, V_{cyl}, as (Fig. 5a):

$$W_C = \gamma_R\left(V_{cap} + V_{cyl}\right) \tag{8}$$

where

$$V_{cap} = \pi\left\{\int_{\sqrt{r^2(1+\sin^2\alpha)-b^2}}^{r}\left(r^2 - y^2\right)dy\right\}$$

$$= \pi\left\{\frac{2}{3}r^3 - r^2\sqrt{r^2(1+\sin^2\alpha) - b^2} + \frac{1}{3}\sqrt{\left[r^2(1+\sin^2\alpha) - b^2\right]^3}\right\} \tag{9}$$

and

$$V_{cyl} = \pi\left\{\left(b^2 - r^2\sin^2\alpha\right)\left(\sqrt{r^2(1+\sin^2\alpha) - b^2} - r\,\sin\alpha\right)\right\}. \tag{10}$$

Combining Eqs. (8), (9), and (10) provides the weight overlying the core:

$$W_C = \gamma_R\pi\left[\left\{\frac{2}{3}r^3 - r^2\sqrt{r^2\left(1+\sin^2\alpha\right) - b^2} + \frac{1}{3}\sqrt{\left[r^2\left(1+\sin^2\alpha\right) - b^2\right]^3}\right\} + \left\{\left(b^2 - r^2\sin^2\alpha\right) \times \left(\sqrt{r^2\left(1+\sin^2\alpha\right) - b^2} - r\,\sin\alpha\right)\right\}\right], \tag{11}$$

and the weight of the rind is simply

$$W_R = W - W_C. \tag{12}$$

4.1.1. Type I

The limit-equilibrium results from this model are shown in Fig. 6. Type I failures are predicted on failure planes inclined at c. 60° (Eq. (4)) in domes with ≤38% core by volume (core radius of ≤72% that of the external radius). Here, the failure plane is assumed to be confined to the largely degassed frictional rind (Fig. 5b). In an idealized sense, the high failure plane inclination seems appropriate for the relatively low volume of Type I collapses (Eq. (4)), and because the volatile-rich core is not breached by failure, explosive events would likely not ensue. Note that the factor of safety for a failure plane of 60° is exactly one for the assumed strengths (Fig. 6). This indicates that failure may or may not occur therefore leaving the possibility for low failure plane inclination/major collapses when the core reaches a sufficient volume proportion.

4.1.2. Types II and III

Following the same idealization, planar Type II and III failures are expected to occur on failure planes inclined at c. 33° with >37–38% core by volume, i.e., a core radius of >72% of the external dome radius (Fig. 6a and c). As the core volume proportion grows past 38%, the factor of safety drops significantly below one, indicating imminent failure of the model. The failure planes for Types II and III collapses intersect the volatile-rich core. Because the core is necessarily breached by the failure plane and depressurization is enhanced (Fig. 5b), the possibility of explosive activity following collapse is elevated. This generalization compares well with the observed explosions following the 17 September 1996 and June to November 1997 collapses (Robertson et al., 1998; Druitt et al., 2002).

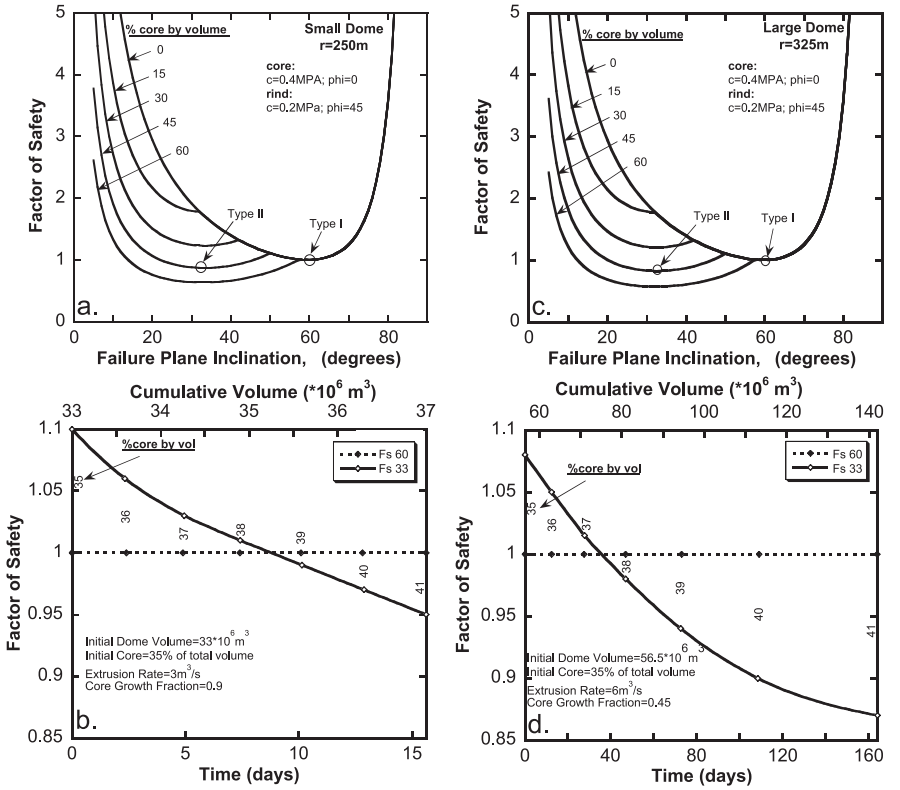

Fig. 6. Illustrations of the limiting equilibriums for idealized hemispherical lava domes comprised of varying amounts of a cohesive core and frictional rind for Types I, II, and III collapses. (a) Small dome (r=250 m). (b) Corresponds to (a); Illustration of the gradual decrease in the minimum factor of safety for failure plane inclinations of 33° (solid line) and the unchanging (F_S=1) minimum factor of safety for those of 60° (dashed line) with increasing core proportion. A switch in critical failure plane inclination from 60° to 33° occurs when the core grows to between 38% and 39% of the dome by volume. (c) Large dome (r=325 m). (d) Corresponds to (c); here, the switch in critical failure plane inclination occurs when the core grows to between 37% and 38% of the dome by volume.

4.2. Retrogressive failure

Some of the major failures, discussed previously, occurred retrogressively, a style not considered in the single-event planar failures described above. Retrogressive instabilities are typified by the collapse of 17 September 1996, which involved repeated failures occurring over a period of 9 h (Calder et al., 2002). The following investigates the potential for retrogressive failure both on circular failure surfaces and as planar slabs, which can ultimately lead to major, potentially explosive, conduit exposing failures.

4.2.1. Circular failure

For a failure to retrogress, several failure surfaces must develop in progression, each successively deeper in the slope than the one preceding. To define the potential for this mode of failure at SHV, a total stress analysis is applied to an inclined slope in cohesive material (φ=0) underlain by a rigid base (Taylor's method; e.g., Fig. 6.9 in Bromhead, 1992). An initial high-angle failure is assumed to transect the frictional rind, and exhume the cohesive core. Subsequent failures occur along successive circular arcs cutting progressively deeper into the exposed slope, and successively flattening the slope face and driving future failure surfaces deeper. The slope height, H, at the threshold of instability may be defined as:

$$H = \frac{c}{N\gamma_R F_S}, \tag{13}$$

where, c is cohesive strength, N is Taylor's stability number, γ_R is the unit weight of the rock, and F_S is the factor of safety, set to unity at the onset of failure.

Table 1 illustrates how failure may progress for a slope comprising a uniform cohesive strength, a frictional strength close to zero, γ_R=26 kN/m^3, with a slope angle that decreases with successive retrogressive collapses. We consider a dome of radius of r=250 m and a cohesion of 1.03 MPa (increased from 0.4 MPa to account for the frictional strength of the rind). After the initial Type I failure removes a volume of ~1.1×10^6 m^3 (assuming 200 m dome thickness), the remnant slope temporarily meta-stabilizes at an inclination prescribed by the strength of the rind material ~60° (see Section 4.1). Subsequent failures occur through the cohesive dome, with average failure surface inclinations extrapolated from the critical failure surfaces corresponding to each successively exhumed slope. Failed volumes are evaluated for particular slope inclinations (Fig. 106 of Hoek and Bray, 1981) by prescribing a nominal friction angle (10°). This evaluated collapse volume, ejected as a pyroclastic flow, is used to update the average slope-face angle for the subsequent retrogressive event. This sequence is repeated until retrogression ultimately arrests. The slope stabilizes as the overall slope successively flattens in response to successive collapses, and the backscarp relief of the failure (Fig. 7) simultaneously diminishes, additively reducing the net forces promoting failure. For the 220-m-high 60° slope, assuming a dome thickness perpendicular to the model section of 200 m, an approximate volume of 3.9×10^6 m^3 would be removed by the second of the three mass movements (Fig. 7). This failure would result in a 250-m-high ~45° slope. Failure of this slope would remove an approximate volume of 5.1×10^6 m^3 (Fig. 7). In total, the retrogressive failure would remove ~10.1×10^6 m^3 including the initial 1.1×10^6 m^3 Type I failure. This is in close agreement with the total volume removed by the 17 September 1996 collapse of 9.5×10^6 m^3 (Calder et al., 2002).

4.2.2. Slab failure in hemispherical domes

Retrogressive failure may also be represented by planar failure modes, using the two-block model illustrated in Fig. 8a. A slope-parallel prism of

Table 1
Height requirements for retrogressive failure calculated from Taylor's curves (Fig. 6.9 of Bromhead, 1992)

Slide #	F_S	Depth factor, D	Slope angle, β	Stability number, N	Required height (m)	Volume removed ($\times10^6$ m^3)
1	–	–	–	–	–	1.1
2	1	1	60°	0.19	208	3.9
3	1	1	45°	0.17	233	5.1
4	1	1	25°	0.135	293	0

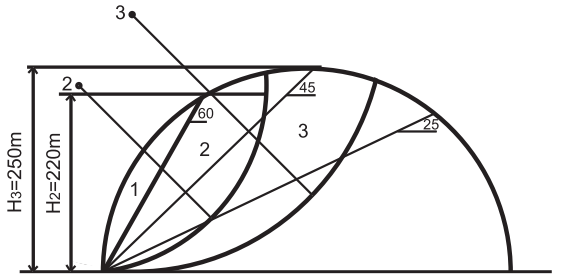

Fig. 7. Diagram of predicted retrogressively developed failure surfaces in a hemispherical dome of r=250 m. Taylor's curves (Fig. 6.9 of Bromhead, 1992) define heights necessary to drive failure, while critical failure surfaces are predicted with Fig. 106 of Hoek and Bray (1981). Area 1 corresponds to the initiating Type I failure. Areas 2 and 3 are the ensuing failures. Retrogression ceases after the third failure because the dome height is no longer capable of driving failure.

thickness y, and height H, is released as a toe-block displaces under gravitational loading. Forces are transmitted be-tween the upper and lower blocks at an angle, δ, pre-scribed by the strength along the interface. Limiting equilibrium of the system (see Appendix A for a de-tailed development) defines a factor of safety, F_S, as:

$$F_S = \{c_2L_2\sin\delta + \sin\delta\cos(180-\alpha-\delta)c_3L_3 + \cos(\alpha-90+\delta)[c_1L_1 + c_3L_3\cos\delta]\} / W_2\sin\delta\sin\alpha, \quad (14)$$

where cohesions, c, act over failure surface lengths, L_1–L_3 (Fig. 8a). For a prescribed slope inclination, a minimum factor of safety is recovered for a critical interblock force inclination, δ, and corresponding to a critical depth of the slope-parallel failure plane, y. As each block fails, the collapse material is ejected from

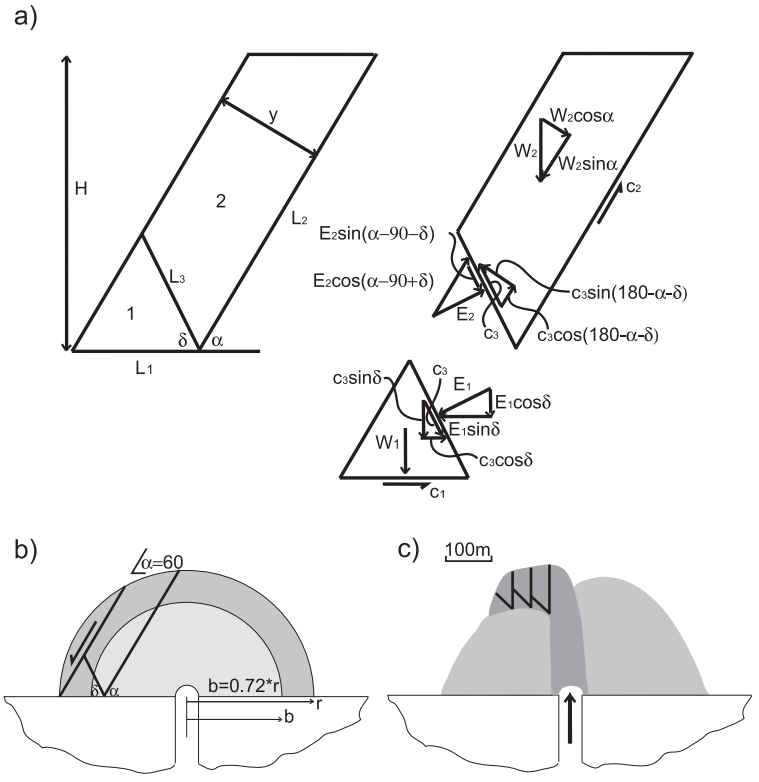

Fig. 8. Schematic diagram of the two-block stability model for retrogressive failure. (a) The free-body diagrams for the two blocks, illustrating the forces acting on each block that are used in the stability model development. (b) The two-block retrogression model embedded in the dual-region hemispherical dome. (c) The two-block retrogression model embedded in the rectangular shear lobe. Each block is separated by a slope-perpendicular tension crack.

the system due to the likely development of pyroclastic flows.

To investigate the potential for retrogressive failure in a hemispherical dome, the two-block model is embedded in the dual-region model developed in Section 4 (Fig. 8b). As with the previous analysis for circular failure surfaces, we assume that the failure sequence initiates with a high-angle planar (Type I) failure through the outer rind, leaving an unprotected cohesive slope inclined at 60°; hence, α is assumed to be 60°. Fig. 9 identifies the critical geometry for a lava dome of r=250 m with c=1.03 MPa (again increased from 0.4 MPa to account for the frictional strength of the rind) after an initiating Type I failure. For an average dome height of 235 m, following removal of the Type I failure, the critical block thickness (corresponding to a minimum factor of safety of unity), y, is 160 m, and the critical slip plane inclination, δ, is 52°.

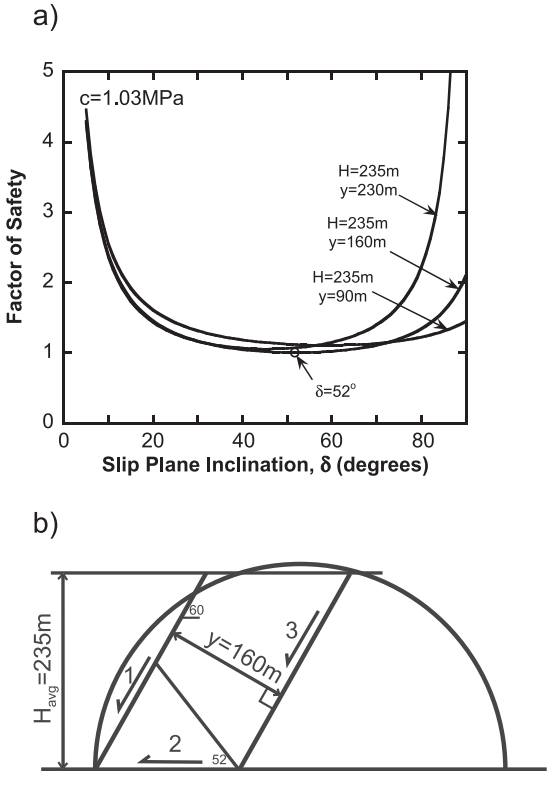

Fig. 9. Illustration of the critical geometry for a dome with r=250 m. (a) The critical slip plane inclination of 52° is identified for the critical block length of 160 m and height of 235 m. (b) Schematic representation of the retrogressive sequence.

After the Type I failure occurs and is removed from the system, one further failure would occur. This second failure would be quite large (Fig. 9b) and would excavate deep into the cohesive core, therefore enhancing depressurization and the likelihood of explosive activity as seen on 17 September 1996 (Watts et al., 2002). Comparing Fig. 9b with Fig. 7, it can be seen that the two-block analysis renders a similar final slope profile to that resulting from collapse on a circular failure surface. For a dome section 200 m along strike, the total volume removed would be ~10.3×10^6 m^3 This is in close agreement with the actual volume removed on 17 September 1996 (9.5×10^6 m^3), and together with the analysis for failure along a circular arc, represents a plausible mechanism for the collapse.

4.2.3. Retrogressive shear lobe failure

Some failures at SHV have been more lobate in form than the deeply incised endogenous dome failures discussed so far (i.e., the failure of 25 June 1997; Watts et al., 2002). These failures can be idealized as two-dimensional rectangular slabs. Here, retrogressive behavior is replicated with the two-block stability model embedded in the idealized rectangular shear lobe, illustrated in Fig. 8c. Observations at SHV (Figs. 9a, 11c, 28e, and 33 of Watts et al., 2002) indicate the presence of subvertical fractures within shear lobes. We assume that these subvertical fractures transect the entire shear lobe, mechanically isolating adjacent blocks, and prescribing compartmental failure geometries.

Fig. 10 identifies the critical slip plane inclination for a reckoned shear lobe geometry of the 17 May 1997 lobe on 23 June 1997, 2 days before the major collapse of 25 June 1997: block length, y=50 m and height, H=110 m. The 17 May 1997 lobe, which was completely removed by the 25 June collapse, is reckoned of total length, width, and height of ~150 m, ~300 m, and ~110 m, respectively (Fig. 35 of Watts et al., 2002). A block length of y=50 m is assumed because the 25 June 1997 collapse was observed to have collapsed as three distinct events.

It can be seen in Fig. 10 that the critical (i.e., minimum F_S value) slip plane inclination, δ, is approximately 42° for the prescribed block isolated

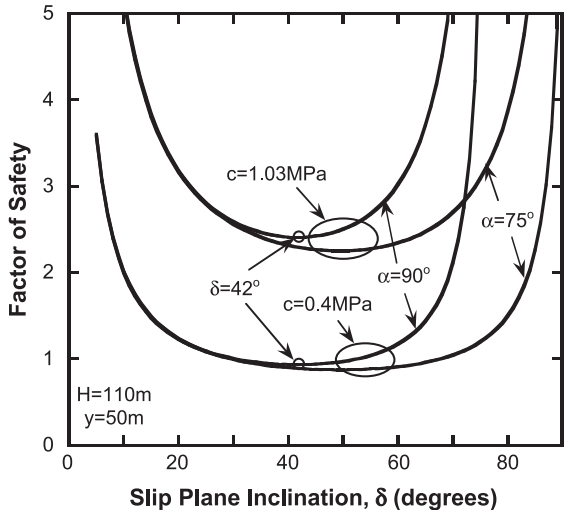

Fig. 10. Graph used to illustrate the method used to find the critical interblock slip plane orientation, δ, for the block length, y=50 m, and height, H=110 m, for the two-block model.

by the slope-perpendicular vertical fractures. However, fracture inclinations of 75° return similar results, indicating a relatively low sensitivity of the α value (Fig. 10). It is important to note that when cohesion of the material is assumed to be 0.4 MPa, the minimum factor of safety is less than one. However, when cohesion is increased to 1.03 MPa to account for the frictional rind, as with the previous calculations, the factor of safety is never less than or equal to one. This analysis indicates that if c=0.4 MPa, failure could occur in three blocks of 50 m length, 300 m width (along strike), and 110 m height each for a total of 5.0×10^6 m^3, and retrogression would terminate due to the topographic limitations at the end of the lobe. Again, this closely corresponds with the actual collapse volume removed on 25 June 1997 of 4.9×10^6 m^3 (Calder et al., 2002).

5. Nested model failure analysis

With failure styles categorized in terms of active mechanisms and controlling strength distributions, we attempt to honor these failure modes with a rational model of dome growth and periodic destruction. We first prescribe the distribution of new lava into the core by partitioning the dome growth into two portions; the fraction effused exogenously to the dome surface, that solidifies and creates a predominantly frictional rind, and the endogenous fraction of growth injected as a soft interior. We then examine stability of the evolving dome to test whether the observed spontaneous switching from high-angle small-to-large failures to low-angle major failures occurs.

5.1. Magma partitioning within the dome

Collapse styles have been shown to switch between high-angle–low-volume (Type I) and low-angle–high-volume (Type II–III) failures as the soft-core interior increases beyond a threshold volumetric proportion. For the assumed model and strength magnitudes, this threshold is ~38% core/62% rind. We may represent growth of the dome by partitioning the distribution of new magma within the dome, that in turn may influence the style of collapse, and the additive involvement of gas overpressures to gravitational forces in promoting extended runout of pyroclastic flows (Fink and Kieffer, 1993). The total volumetric dome-growth rate, $\dot{E}$, may be partitioned between the fraction injected into the core, ε_C, and the fraction effused to the rind, ε_R. Assuming these fractions to remain constant in time, the dome volume, V_f, may be defined at any time, Δt, as:

$$V_f = \left[\left(\varepsilon_C \times \dot{E}\right) + \left(\varepsilon_R \times \dot{E}\right)\right]\Delta t - V_{collapse} + V_i, \tag{15}$$

in terms of initial volume, V_i, and the volume removed by periodic collapse, $V_{collapse}$. With the assumptions of initial core, v_i^C, and rind, v_i^R, fractional volume proportions and actual volumes of core, $V^C_{collapse}$, and rind, $V^R_{collapse}$, removed by failure, it is straightforward to calculate the final fractional core, v_f^C, and rind, v_f^R, proportions as:

$$v_f^C = \frac{\left[\varepsilon_C\left(\dot{E}\right) - V^C_{collapse} + v_i^C(V_i)\right]}{V_f} \tag{16}$$

and

$$v_f^R = 1 - v_f^C. \tag{17}$$

5.2. Single-event failures in small domes

Fig. 6b illustrates the idealized progression of a small dome (r=250 m) from Type I failures to Type II

failures assuming that at an arbitrary time zero the dome contains 35% core by volume and has a total volume of 33×10^6 m^3, an extrusion rate of 3 m^3/s, ε_C=0.9, and no lava is lost due to failures during the time period. The high value of ε_C is chosen for two reasons: (1) failure timing (discussed below) corresponds best with ε_C=0.9, and (2) Kaneko et al. (2002) have shown that in general, slow extrusion rates favor endogenous growth at Unzen volcano in Japan. Watts et al. (2002) suggest an apparent contradiction of this for SHV where slow extrusion favors the expulsion of crystalline rigid lobes. This observation could be interpreted as slow infusion favoring exogenous growth; however, the lobe is merely the ultimate surface expression of infusion of soft volatile-rich material to the dome core, and is only apparent as the carapace is ultimately breached. Thus, endogenous growth can feasibly occur even as lobes simultaneously pierce the surface. Even after lobe extrusion, the root of the shear lobe is shielded from degassing by its depth within the core, remains soft, and may form the essential component for a deeply diving shear failure. Consequently, the observed expulsion of lobes is compatible with the concurrent growth of the dome interior that drives this periodic lobe expulsion. Even as the lobe pushes to the surface, continued endogenous growth must continue at least until another shear lobe is formed, still resulting in a large proportion of endogenous growth.

Specifically, Fig. 6b shows the gradual decrease in the factor of safety for failure plane inclinations of 33° and the unchanging factor of safety (equal to one) for failure planes inclined at 60°, corresponding to increasing dome volume and core proportion. As the dome grows beyond 38% core by volume, the critical failure mode switches directly from high-angle (60°) to low-angle (33°) collapse. This results from the low-angle plane (F_S<1) becoming less stable than the high-angle plane (F_S=1) due to the decreased strength corresponding to the increased core proportion of the potential 33° failure plane relative to the potential 60° failure plane. This drastic change in collapse style from Type I to Type II failures occurs over a period of days with no change in behavior on the dome interior, which qualitatively matches the actual collapse of 17 September 1996. There was a 2-week period prior to 17 September 1996 marked by the absence of significant collapse activity culminating in the 9-h continuous collapse that removed c. 35% of the dome (Watts et al., 2002; Calder et al., 2002).

5.3. Single-event failures in large domes

Fig. 6d illustrates the idealized progression of a large dome (r=325 m) from Type I to Type III failures assuming an initial dome volume of 56.5×10^6 m^3, an extrusion rate of 6 m^3/s, ε_C=0.45, and again with 35% core by volume initially and no lava lost due to failures during the time period. The lower value of ε_C is chosen to best replicate failure timing, but is also consistent with rapid extrusion rates generally favoring exogenous growth (Kaneko et al., 2002). Here, the abrupt switch in failure style occurs as the proportion of soft dome core grows beyond ~37% of the total, again with no imposed change in growth behavior (Fig. 6d). Again, there is a qualitative correspondence with timing of the collapse of 25 June 1997. The time between the last Type I failure and the first Type III failure is approximately 1.5 months, which correlates well with the collapse hiatus between April and June 1997 (Calder et al., 2002).

6. Model implications and limitations

The simple dual region model of a cohesive core and frictional rind seems to explain how the collapse mechanism of a lava dome may evolve from high-angle–low-volume (Type I) collapses to more hazardous low-angle–high-volume (Type II or III) failures with no change in system forcing, viz., the lava injection rate. Importantly, because this occurs with no apparent change in the magma injection rate, the transformation to a more hazardous collapse style is not heralded by a precursory signature. For the dual-region model, the change in collapse style is shown to evolve naturally as the soft core grows to a critical volume proportion. For the particular idealization of a hemispherical dome, and assumed strength magnitudes, this threshold core volume is ~37–39% of the total dome. With little warning, one dominant failure style can be overcome by another more dramatic and hazardous style. This transition represents a bifurcation point, where at the threshold geometry both high- and low-angle failures are equally likely to occur. Unfortunately, this model does not define a rigorous

method to predict failure style because determining with certainty what portions of growth are adding to the core and rind is extremely difficult. However, it does provide a reasonable explanation of past behavior at SHV.

The dual-region model provides some insight into how the various recognized collapse styles may develop; however, it does have some limitations. The strength magnitudes are approximate and may not match the strength distributions in actual lava domes. Sparks et al. (2000) performed creep tests on dome rocks at 993 °C. The intact samples failed under a load of 9.1 MPa, which provides an upper strength bound for the cohesive core material. When this strength is applied to the core in the dual-region model, low-angle failure never develops because the rind is always much weaker, placing the failure plane at 60°. Furthermore, in reality, the SHV lava dome does not typically grow equidimensionally as a hemisphere as in the model. Growth generally occurs in focused regions of the dome, thus the growth rates cause more significant localized topographic changes in the real dome in a shorter amount of time than in the model.

Although the retrogressive models involving circular failure include significant uncertainties, they provide an important implication. This is that according to the calculations, in order for retrogression to develop, local slope height must increase for each retrogressive episode to develop. With the hemispherical geometry assumed, this is possible until the rear scarp of the failure passes beyond the dome crest, terminating the retrogression. In addition, the two-block slab models provide quantification of another potential retrogressive mechanism. Importantly, the analyses of retrogressive failure by both circular and planar modes return similar results; these qualitatively honor the sequence and style of collapse events, despite the general lack of available data on material strengths and individual failure surface geometries.

All of the analyses neglect the potential for additional triggering agents, such as lava movement, internal gas pressurization, seismic acceleration, and quenching by precipitation. Importantly, these additional triggers are not needed to cause the observed and systematic switch in failure mode from shallow to deep-seated failure, although conceivably they may act to varying degrees. The observed switching in failure was not correlated with obvious seismic or rainfall triggering. Gas pressurization has been shown to drive a similar transition from shallow to deeper failures (Voight and Elsworth, 2000; Elsworth and Voight, 2001), although typically with a related growth in the intensity of seismic activity immediately preceding failure. This signature is absent in the events documented here, and the failures correspondingly occur with little warning and absent significant precursors.

7. Conclusions

The systematic evolution of dome collapse style described here facilitates understanding some of the fundamental processes that take place within an actively growing andesite lava dome. Although no simplification of such a complex system can be used to explain all details, the apparently chaotic behavior of dome collapses can be explained logically by relatively simple means. Of the four collapse styles, Type III collapses are by far the most hazardous as they occur rapidly and can result in violent explosions, sometimes within minutes after the onset of collapse. The precursory activity that takes place prior to Type III collapses, i.e., rapid extrusion, cyclic tilt, intense hybrid earthquakes, etc., provides clear warnings of forthcoming activity. However, Type II collapses are rather problematic in that the transition from Type I is not well defined. Type I collapses are relatively common and similar in size to the less common Type IV collapses involving soft pancake-like lobes. However, their mechanisms seem to be quite different.

By idealizing lava domes as hemispheres with two discrete regions, a frictional outer rind surrounding a cohesive gas-rich core, this work has shown that both small-to-large and major failures can occur in domes comprised of nearly equal core/rind volume proportion. Differential growth between the core and rind allows for the relative growth of one or the other by only a few percent allowing, again in idealized form, the various recognized collapse styles to develop. Importantly, the feasibility of a bifurcation point between small-to-large and major collapses has been established, suggesting that indiscernible internal fluctuations might determine whether small-to-large

or major collapses will occur when the core comprises some threshold volume proportion.

Importantly, two end-member styles of major failure development have been proposed and explored, i.e., single-event planar failure and multi-event retrogressive failure. These correspond to observed short- and long-duration collapses, respectively. The retrogressive models specifically aid in the explanation of the 17 September 1996 collapse that occurred over a period of c. 9 h and the 25 June 1997 collapse that is thought to have occurred in three individual collapses. Two plausible explanations of retrogressive failures have been suggested. These are the retrogressive failure on circular detachment planes, driven by increasing slope height, and ultimately arresting as slope angles flatten and backscarp elevation ultimately drops. And, the retrogressive failure of slope-parallel prismatic slabs that develop on release surfaces provided by slope-perpendicular release planes. These mechanisms have not been analyzed rigorously but do provide some insight into possible retrogressive failure scenarios.

Symbol explanations

Symbol	Property (Units)
c	Cohesion (MPa)
c_C	Cohesion of core material (MPa)
c_R	Cohesion of rind material (MPa)
φ	Friction angle (°)
φ_C	Friction angle of core material (°)
φ_R	Friction angle of rind material (°)
F_S	Factor of safety
r	Outer dome radius (m)
b	Dome core radius (m)
α	Failure plane inclination (°)
A	Total area of failure plane (m^2)
A_C	Area of failure plane overlying core (m^2)
A_R	Area of failure plane overlying rind (m^2)
W	Total failure block weight (N)
W_C	Failure block weight overlying core (N)
W_R	Failure block weight overlying rind (N)
V	Failure block volume (m^3)
V_{cap}	Failure block volume overlying core; cap portion (m^3)
V_{cyl}	Failure block volume overlying core; cylindrical portion (m^3)
γ_R	Unit weight of rock (N/m^3)
Δt	Elapsed time (days)
$\dot{E}$	Extrusion rate (m^3/s)
ε_C	Proportion of extruding lava accruing to core
ε_R	Proportion of extruding lava accruing to rind
$V_{collapse}$	Volume of dome rock removed by collapse (m^3)
V_i	Total initial dome volume (m^3)
V_f	Total final dome volume (m^3)
v_i^C	Initial core volume proportion (of total dome volume)
v_i^R	Initial rind volume proportion (of total dome volume)
$V_{collapse}^C$	Volume of core removed by collapse (m^3)
$V_{collapse}^R$	Volume of rind removed by collapse (m^3)
v_f^C	Final core volume proportion (of total dome volume)
v_f^R	Final rind volume proportion (of total dome volume)
q_D	Darcian velocity (m/s)
k	Bulk permeability (m^2)
μ	Fluid viscosity (Pa·s)
Δp	Pressure gradient
L	Drainage path length (m)
E_1	Force acting on block 1 normal to slip plane (N)
E_2	Force acting on block 2 normal to slip plane (N)
δ	Slip plane inclination (°)
L_1	Length along block 1 basal release surface (m)
L_2	Length along block 2 subvertical release surface (m)
L_3	Length of interblock slip plane (m)
c_1	Cohesion acting along L1, basal surface (MPa)
c_2	Cohesion acting along L2, subvertical surface MPa)
c_3	Cohesion acting along L3, interblock surface (MPa)
W_2	Weight of failure block 2 (N)
V_1	Volume of failure block 1 (m^3)
V_2	Volume of failure block 2 (m^3)
V_{total}	Total volume of failure blocks 1 and 2 (m^3)
N	Taylor's stability number
H	Slope height (m)
y	Length of blocks (retrogression model) (m)

Acknowledgements

This work is a result of partial support by the U.S. National Science Foundation under grant CMS-9908590. This support is gratefully acknowledged. The contribution of Hide Yasuhara to the derivation of stability relations is gratefully acknowledged.

Appendix A. Development of the two-block stability model

For the geometry illustrated in Fig. 8a, the forces acting on block 1 parallel to L_1 assuming a purely cohesive rock mass are:

$$E_1\sin\delta = \frac{c_1L_1}{F_S} + \frac{c_3L_3\cos\delta}{F_S}, \tag{A-1}$$

and the forces acting on block 2 parallel to L_2 are:

$$W_2\sin\alpha - E_2\cos(\alpha - 90 + \delta) = \frac{c_2L_2}{F_S} + \frac{c_3L_3\cos(180 - \alpha - \delta)}{F_S}, \tag{A-2}$$

where E_1=E_2 is the interblock force, F_S is the factor of safety, c is cohesive strength, W is block weight, and all other symbols are identified in Fig. 8a. Solving for E_1 and E_2 gives:

$$E_1 = \frac{c_1L_1 + c_3L_3\cos\delta}{F_S\sin\delta}, \tag{A-3}$$

and

$$E_2 = \frac{W_2\sin\alpha - \frac{c_2L_2}{F_S} - \frac{c_3L_3\cos(180-\alpha-\delta)}{F_S}}{\cos(\alpha - 90 + \delta)}. \tag{A-4}$$

Setting E_1 equal to E_2 (necessitated by statics) allows for the true factor of safety to be identified as:

$$F_S = \frac{c_2L_2\sin\delta + \sin\delta\cos(180 - \alpha - \delta)c_3L_3 + \cos(\alpha - 90 + \delta)[c_1L_1 + c_3L_3\cos\delta]}{W_2\sin\delta\sin\delta}. \tag{A-5}$$

The lengths L_1, L_2, and L_3 are found trigonometrically as:

$$L_1 = \frac{\gamma}{\sin\alpha}, \tag{A-6}$$

$$L_2 = \frac{H}{\sin\alpha}, \tag{A-7}$$

when $\delta<90-\alpha$

$$L_3 = \frac{\gamma}{\cos((90 - \alpha) - \delta)}, \tag{A-8}$$

and when $\delta\geq90-\alpha$

$$L_3 = \frac{\gamma}{\cos(\delta - 90 + \alpha)}, \tag{A-9}$$

where y is the length of the blocks, and H is the slope height as illustrated in Fig. 8. The weight of block 2 is calculated through its volume, V_2, and unit weight, γ_R=26 kN/m^3, as:

$$W_2 = \gamma_R V_2 = \gamma_R(V_{total} - V_1), \tag{A-10}$$

where

$$V_{total} = \left\{ y\left[\left(\frac{H}{\sin\alpha}\right) - \left(y\frac{\cos\alpha}{\sin\alpha}\right)\right] + \left[y^2\left(\frac{\cos\alpha}{\sin\alpha}\right)\right]\right\} \times 1 \text{ unit thick.} \tag{A-11}$$

When $\delta\geq90-\alpha$

$$V_1 = \left\{ \frac{1}{2}y\left[\left(y\frac{\cos\alpha}{\sin\alpha}\right) + y\tan(\delta - (90 - \alpha))\right]\right\} \times 1 \text{ unit thick,} \tag{A-12}$$

and when $\delta<90-\alpha$

$$V_1 = \left(\frac{1}{2}\frac{y}{\sin\alpha}\frac{y}{\sin(\alpha + \delta)}\sin\alpha\right) \times 1 \text{ unit thick.} \tag{A-13}$$

References

Bromhead, E.N., 1992. The Stability of Slopes. 2nd ed. Blackie Academic and Professional, London, 411 pp.

Calder, E.S., Luckett, R., Sparks, R.S.J., Voight, B., 2002. Mechanisms of lava dome instability and generation of rockfalls and pyroclastic flows at Soufrière Hills Volcano, Montserrat. In: Druitt, T.H., Kokelaar, B.P. (Eds.), The Eruption of Soufrière Hills Volcano, Montserrat, from 1995 to 1999. Memoirs. Geological Society, London, 21, 173–190.

Crowley, J., Zimbelman, D., 1997. Mapping hydrothermally altered rocks on Mount Rainier, Washington, with Airborne Visible/Infrared Imaging Spectrometer (AVIRIS) data. Geology 25, 559–562.

Druitt, T.H., Young, S.R., Baptie, B., Bonadonna, C., Calder, E.S., Clarke, A.B., Cole, P.D., Harford, C.L., Herd, R.A., Luckett, R., Ryan, G., Voight, B., 2002. Episodes of cyclic Vulcanian explosive activity with fountain collapse at Soufrière Hills Volcano, Montserrat. In: Druitt, T.H., Kokelaar, B.P. (Eds.), The Eruption of Soufrière Hills Volcano, Montserrat, from 1995 to 1999. Memoirs. Geological Society, London, 21, 173–190.

Elsworth, D., Voight, B., 2001. The mechanics of harmonic gas pressurization and failure of lava domes. Geophysical Journal International, Royal Astronomical Society 145, 187–198.

Elsworth, D., Voight, B., Thompson, G., Young, S.R., 2004. A thermal-hydrologic for rainfall-triggered collapse of lava domes. Geology, In press, 20 pp.

Fink, J., Griffiths, R., 1998. Morphology, eruption rates, and rheology of lava domes: insights from laboratory models. Journal of Geophysical Research 103 (B1), 527–545.

Fink, Kieffer, 1993. Estimate of pyroclastic flow velocities resulting from explosive decompression of lava domes. Nature 363 (6430), 612–615.

Hale, A., Wadge, G., 2003. Numerical modeling of the growth dynamics of a simple silicic lava dome. Geophysical Research Letters 20, 19.

Hoek, E., Bray, J., 1981. Rock Slope Engineering, 3rd ed. Institution for Mining and Metallurgy, E and FN Spon, 358 pp.

Iverson, R.M., 1990. Lava domes modeled as brittle shells that enclose pressurized magma, with application to Mount St. Helens. In: Fink, Jonathan H. (Ed.), Lava Flows and Domes, Emplacement Mechanisms and Hazard Implications. Springer Verlag, Berlin, pp. 47–69.

Kaneko, T., Wooster, M., Nakada, S., 2002. Exogenous and endogenous growth of the Unzen lava dome examined by satellite infrared image analysis. Journal of Volcanology and Geothermal Research 116, 151–160.

Lopez, D., Williams, S., 1993. Catastrophic volcanic collapse: relation to hydrothermal processes. Science 260, 1794–1796.

Matthews, A.D., Barclay, J., 2004. A thermodynamical model for rainfall-triggered volcanic dome collapse. Geophys. Res. Lett. 31(5), No. L05614 MAR 12 2004.

McGuire, B., Norton, G., Sparks, R.S.J., Robertson, R., Young, S., Miller, A., 1996. Report of the Explosive Event of 17–18 September 1996, Montserrat Volcano Observatory Special Report 1. Montserrat Volcano Observatory, Digital Elevation Maps from November 1995–March 1998 time period.

Robertson, R., Cole, P., Sparks, R.S.J., Harford, C., Lejeune, A.M., McGuire, W., Miller, A., Murphy, M., Norton, G., Stevens, N., Young, S., 1998. The explosive eruption of Soufrière Hills volcano, Montserrat, West Indies, 17 September, 1996. Geophysical Research Letters 25, 3429–3432.

Robertson, R., Aspinall, W., Herd, R., Norton, G., Sparks, R., Young, S., 2000. The eruption of the Soufrière Hills volcano, Montserrat, W.I. Philosophical Transactions of the Royal Society of London 358, 1619–1637.

Simmons, J., Elsworth, D., Voight, B., 2004. Instability of exogenous lava lobes during intense rainfall. Bull. Volc. DOI:10.1007/s00445-004-0353-y.

Sparks, R.S.J., Young, S.R., 2002. The eruption of the Soufrière Hills Volcano, Montserrat (1995–1999): overview of scientific results. In: Druitt, T.H., Kokelaar, B.P. (Eds.), The Eruption of Soufrière Hills Volcano, Montserrat, from 1995 to 1999, Memoirs, vol. 21. Geological Society, London, pp. 45–69.

Sparks, R.S.J., Murphy, M.D., Lejeune, A.M., Watts, R.B., Barclay, J., Young, S.R., 2000. Control on the emplacement of the andesite lava dome of the Soufrière Hills Volcano, Montserrat, by degassing-induced crystallization. Terra Nova 12, 14–20.

Voight, B., Elsworth, D., 1997. Failure of volcano slopes. Geotechnique 47 (1), 1–31.

Voight, B., Elsworth, D., 2000. Instability and collapse of hazardous gas-pressurized lava domes. Geophysical Research Letters 27 (1), 1–4.

Voight, B., Hoblitt, R.P., Clarke, A.B., Lockhart, A.B., Miller, A.D., Lynch, L., McMahon, J., 1998. Remarkable cyclic ground deformation monitored in real time on Montserrat and its use in eruption forecasting. Geophysical Research Letters 25, 3405–3408.

Voight, B., Komorowski, J.-C., Norton, G.E., Belousov, A.B., Beousova, M., Boudon, G., Francis, P.W., Franz, W., Heinrich, P., Sparks, R.S.J., Young, S.R., 2002. The 26 December (Boxing Day) 1997 sector collapse: a case history from Soufrière Hills Volcano, Montserrat. In: Druitt, T.H., Kokelaar, B.P. (Eds.), The Eruption of Soufrière Hills Volcano, Montserrat, from 1995 to 1999. Memoirs. Geological Society, London, 21, 363–407.

Watters, R., Zimbelman, D., Bowman, S., Crowley, J., 2000. Rock mass strength assessment and significance to edifice stability, Mount Ranier and Mount Hood, Cascade Range volcanoes. Pure Applied Geophysics 157, 957–976.

Watts, R.B., Herd, R.A., Sparks, R.S.J., Young, S.R., 2002. Growth patterns and emplacement of the andesitic lava dome at Soufrière Hills Volcano, Montserrat. In: Druitt, T.H., Kokelaar, B.P. (Eds.), The Eruption of Soufrière Hills Volcano, Montserrat, from 1995–1999. Geological Society, London, Memoirs, 21, 115–152.

Yamasato, H., Kitagawa, S., Komiya, M., 1998. Effect of rainfall on dacitic lava dome collapse at Unzen volcano, Japan. Papers in Meteorology and Geophysics 48 (3), 73–78.